N94-33296

DESIGN, CHARACTERIZATION AND CONTROL OF THE UNIQUE MOBILITY CORPORATION ROBOT

Virgilio B. Velasco, Jr., and Wyatt S. Newman
Case Western Reserve University
Cleveland, Ohio

Bruce Steinetz
NASA Lewis Research Center
Cleveland, Ohio

and

Carlo Kopf and John Malik*
Unique Mobility, Inc.
Golden, Colorado

Abstract

Space and mass are at a premium on any space mission, and thus any machinery designed for space use should be lightweight and compact, without sacrificing strength. It is for this reason that NASA/LeRC contracted Unique Mobility Corporation to exploit their novel actuator designs to build a robot that would advance the present state of technology with respect to these requirements. Custom-designed motors are the key feature of this robot. They are compact, high-performance dc brushless servo motors with a high pole count and low inductance, thus permitting high torque generation and rapid phase commutation. Using a custom-designed digital signal processor-based controller board, the pulse width modulation power amplifiers regulate the fast dynamics of the motor currents. In addition, the programmable digital signal processor (DSP) controller permits implementation of nonlinear compensation algorithms to account for motoring vs regeneration, torque ripple, and back-EMF. As a result, the motors produce a high torque relative to their size and weight, and can do so with good torque regulation and acceptably high velocity saturation limits. This paper presents the Unique Mobility Corporation robot prototype: its actuators, its kinematic design, its control system, and its experimental characterization. Performance results, including saturation torques, saturation velocities and tracking accuracy tests are included.

1 Introduction

The Unique Mobility Corporation (UNIQ) robot is a mechanical arm whose construction was commissioned by the NASA Lewis Research Center, under a small business innovative research contract [1]. It is a compact, powerful, lightweight robot designed for possible use in space applications, where space and mass are at a premium. The purpose of this project

*In memoriam.

PRECEDING PAGE BLANK NOT FILMED

was to construct high torque-to-mass density actuators based on the high pole-count Unique Mobility design, compare relative performance of these actuators to competing industrial servomotors, and implement the actuators into a light-weight three-axis robot arm and evaluate their installed performances. This report provides an overview of the project findings and indicates methods by which the robot actuator performances can be improved.

2 General Characteristics of the Robot Arm

The robot has several unique design features.

To save weight without sacrificing stiffness, the links were constructed using a composite of carbon fibers interlaced through an epoxy matrix, instead of using aluminum or steel. This makes it much lighter than aluminum, with much of the strength of steel[2, 3, 4, 5, 6].

The robot uses three compact, high torque-to-mass density three-phase brushless DC motors custom-designed by Unique Mobility Corporation. Wasted space was minimized by fully integrating the sensors, rotor and harmonic drive, resulting in a highly compact design. Each motor has about twice the torque-to-mass ratio of existing servo motors, as will be discussed. They have a high pole count and low phase inductances, which allow high torque generation and rapid commutation [7]. They also have a full complement of sensors: thermal sensors, a motor resolver and two output shaft resolvers (one for coarse angle measurements, one for finer measurements). While the motor resolver reports the angular position of the motor shaft itself (i.e. before the harmonic drive), the output resolvers sense the joint angle, or the position of the shaft after the harmonic drive.

Each motor is connected to a sophisticated controller card which uses surface-mount technology to incorporate features in a compact assembly. Each card has its own microprocessor (an N80C196KC chip), on-board memory and I/O processing devices. The digital signal processor-based cards [8] are responsible not only for motor commutation and current control, but for such tasks as sensor output processing and back-EMF compensation. These features are discussed more thoroughly in Section 3.3.

Output torque is sensed through a custom designed torque sensor that can be used for torque feedback control. The torque sensor consists of a spoked-wheel driven at its hub by the harmonic drive output and connected to the robot link at its outer ring. Calibrated strain gages mounted on the root of the structurally optimized spokes provides the desired torque signal.

3 Hardware Description

3.1 Motor Design and Performance

As explained above, the UNIQ motor was designed to have a high power density and high torque to mass ratio. To demonstrate that these goals were achieved, the UNIQ motor

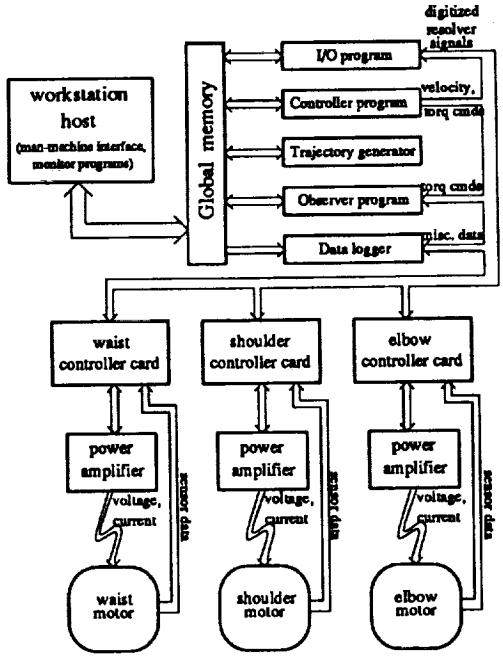

Figure 1: Hardware block diagram

was compared to two similar actuators on the market. The other motors were chosen to have similar torque limits as the UNIQ motor (about 400 $N \cdot m$). However, this is where the similarities end.

The comparison is not a direct one as the UNIQ motor was designed to be used with a harmonic drive which is limited to 2000 rpm and the other motors were not. The other motors will produce much more power for the same amount of torque simply because of the increased speed. In addition, this implies that the other motors have a lower back EMF constant, and thus, a lower torque constant. As a result, the other motors require more current and generate more heat due to I^2R losses.

Another difference is the packaging of the motors. The UNIQ motor has a larger diameter, and has a cavity in the center which is used to house other mechanical components. The other motors, on the other hand, are designed as compact, stand alone units. The UNIQ motor was designed with a specific application in mind, the 3 degree of freedom arm. Therefore a direct comparison shows the UNIQ motor is penalized by the greater diameter and volume as well as the additional weight due to the larger structural components. The additional torque available due to the UNIQ motor's 1:100 harmonic drive ratio is a distinct advantage in the torque density comparison, without the adjustments discussed below.

Yet another difference lies in the environments the motors are designed to work in. The UNIQ motor was designed for a space environment where the heat rejection would

be by radiation only. The other motors were designed for use in the atmosphere, where convection also helps cool the motors. In order to make an equal comparison, the other motors' torque (at 2000 rpm) was derated by the ratio of the temperature rise of the UNIQ motor (60°C) divided by the other motors' temperature rise (90°C).

The torque figures used for the UNIQ motor have not been adjusted to remove the frictional torque from the oversized bearings as well as the friction from the harmonic drive.

Because of these inequities we have shown two comparisons. The first one is a direct system comparison ignoring all of the inconsistencies (Table 1). The second comparison is a motor only comparison using only the torque producing components (TPC) and constraining the other motors to run at 2000 rpm and to run at a derated torque level due to the temperature (Tables 2 & 3). The harmonic drive has been removed from the volume, weight, and torque output of the UNIQ motor.

The motors used in this comparison were the Industrial Drives model #B-104-A-22 (henceforth referred to as the I.D. motor), and the Pacific Scientific model #R32GENC-R2-NS-NV-00 (the Pac Sci motor).

Table 1: Direct motor comparison

	I.D. motor	Pac Sci motor	UNIQ motor
Total Mass (kg)	3.02	3.13	8.62
Total Torque ($N \cdot m$)	0.0467	0.0467	4.92
Total Speed (rad/s)	590.0	470.0	2.09
Total Power (W)	881	707	331
Total Volume (m^3)	0.00118	0.00124	0.00221
Total Power Density (W/m^3)	747,000	570,000	150,000
Total Torque Density (N/m^2)	39.6	37.7	2230
Efficiency (%)	72.0	74.7	?

Table 2: Torque producing components (motor only) comparison

	I.D. motor	Pac Sci motor	UNIQ motor
TPC Mass (kg)	1.45	1.68	1.16
TPC Volume (m^3)	0.000305	0.000331	0.000270

As was expected the direct system comparison of the power density of both the I.D. and Pac Sci motors were much greater than the UNIQ motor, because of the extra power

Table 3: Derated output for temperature and lower speed

	I.D. motor	Pac Sci motor	UNIQ motor
Continuous Power (W)	210	210	331
Continuous Stall Torque ($N \cdot m$)	0.0703	0.0643	0.105
TPC Power Density (W/m^3)	689,000	634,000	1,230,000
TPC Torque Density (N/m^2)	230	194	389
TPC Power/Mass (W/kg)	144	125	285
TPC Torque/Mass ($N \cdot m/kg$)	0.0485	0.0383	0.0905

due to the increased speed and smaller volume due to the compact design. Obviously the UNIQ motors' torque density was much larger due to the harmonic drive.

Once the motors were compared on a more equal, torque producing component basis, we see that the UNIQ motors' power density and torque density are greater than the I. D. and Pac Sci motors. The power to mass ratio of the UNIQ motor is 1.9 times greater than the I.D motor and 2.3 times greater than the Pac Sci motor. The torque to mass ratio of UNIQ's motor is 1.9 times greater than the I.D. motor and 2.4 times greater than the Pac Sci motor.

3.2 Robot Arm Geometry

The arm itself has three degrees of freedom. Each of its three links is driven at the joint by a small but powerful high-performance motor. Joints 1, 2 and 3 are referred to as the "waist," "shoulder," and "elbow," respectively. The robot arm is designed to move payloads of up to 15 Kg at a reach of 1 meter at speeds of up to 2 m/s at the robot wrist.

3.3 Controller Cards

The joint controller cards handle many different tasks. First, the cards are responsible for reading the various sensor signals and converting them to digital form. These sensors comprise the motor shaft (or input) resolver, the coarse and fine output resolvers and temperature sensors on the motors, the strain gages, and the bus voltage and current sensors on the power amplifiers. The digitized readings are stored in a structure on the card's on-board memory, which can be read by programs running on either the host computer or the CPU cards connected to the VME interface (see Section 3.4).

Second, the cards handle motor commutation. That is, they accept torque commands from the controller program support module (see Section 4.1 for details), and control the phase currents based on the resolver signals.

Third, the cards also function as motor current controllers. Using proportional and integral feedback, they make sure that the actual current closely follows the desired current.

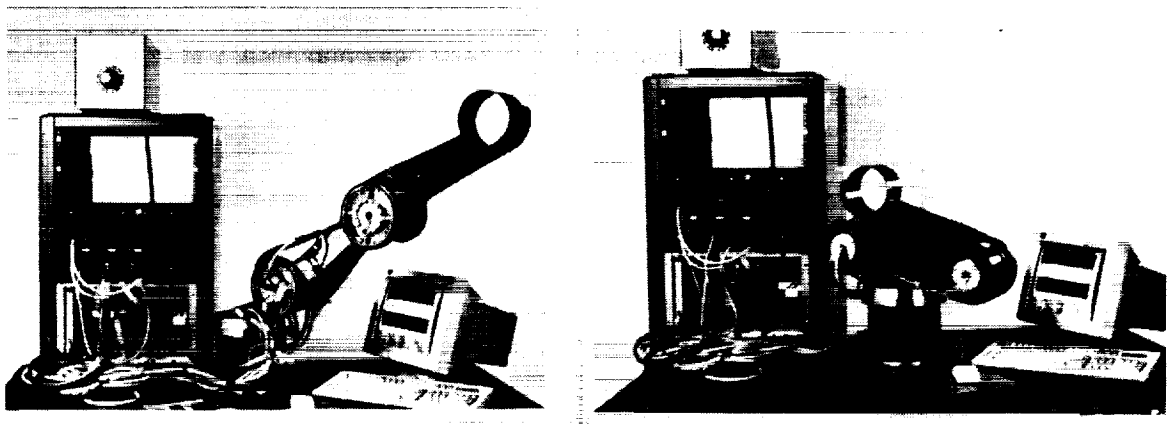

Figure 2: The UNIQ robot arm, controller rack and man-machine interface. Robot fully extended (left) and in stowed position (right)

Their fourth function is to handle switching over from torquing to braking. When the motors are being accelerated, power is delivered from the amplifiers (see Section 3.5) to the motors. During deceleration though, power is regenerated, or transferred back to the amplifiers. To prevent amplifier overload, this power is dumped into several ceramic load resistors instead. The controller cards are responsible for determining when this switching should occur, and for shunting the power into the resistors.

Finally, the cards are responsible for reporting any errors that may occur in torque generation. For instance, if the amount of torque requested exceeds the motor limit, or if a power amplifier appears to be off, the cards report a fault status by setting a variable in their on-board memory. This fault status can thus be detected by other programs on the host or on the VME cage.

3.4 VME interface

To maximize the software's speed and effectiveness, several of the processes must be executed in parallel [9, 10]. The VME interface makes this possible [11, 12].

This interface connects the host computer to a VME card cage. The host is a Sun workstation running UNIX, which serves as the man-machine interface. The card cage, on the other hand, carries several single-board computers (henceforth referred to as "CPU cards") and the aforementioned joint controller cards.

The card cage permits the host, CPU cards and controller cards to communicate with each other. This is done by allowing the host and CPU cards to read and write to the

memory on board both the controller cards and other CPU cards.

The cage uses six CPU cards. Four of these are reserved for the various support modules (see Section 4.1 for details). The fifth is used for the data logging process. The last one functions as a global storage location for variables that are accessed by multiple processes.

3.5 The Power Amplifiers

Each of the three controller cards is connected to a pulse width modulation (PWM) power amplifier, [7, 14, 13] which is in turn connected to one of the motors. These amplifiers are responsible for generating the current which drives the motors. They are also responsible for shorting the motor phases together, when the power is turned off. This effectively acts as a brake, preventing the robot from falling rapidly under gravity loads with the amplifiers off. It is recognized that additional mechanical braking will be required in service.

The controller program support module on one of the CPU cards (Section 4.1) computes the three desired joint torques, and stores these values at designated addresses on the controller cards' dual-port RAM. The cards then perform the motor commutation (as explained earlier in Section 3.3), ordering the amplifiers to produce the proper currents.

4 Software Description

4.1 Support Modules

The software interface to the robot can be divided into five components. The highest-level module, the man-machine interface, runs on the host computer. It is supported by four more modules, which require much more computational speed. These programs run on separate CPU boards in the VME cage.

The I/O program's purpose is to report the motor shaft angles and velocities as quickly and as efficiently as possible. The angles are computed by monitoring the motor resolver readings and the number of rotor revolutions, from which the motor shaft angles can be computed. The velocity can be computed in any of three ways: (1) through raw differentiation of the shaft angle, (2) by digitally filtering the results of this raw differentiaton, to produce a smoother velocity estimate, or (3) by using the velocity estimates returned by the observer program. Under normal operation, the observer-estimated velocity would be used, since it produces the smoothest, most reliable results [17].

The controller program uses a combination of servo control and feedforward torques to make the robot follow its prescribed trajectory. To compute these torques, it uses the actual angles and velocities reported by the I/O program, as well as the desired angles, velocities and accelerations computed by the trajectory generator.

The observer uses the commanded torques and a model of the robot dynamics to estimate the joint velocities. This produces a much smoother velocity estimate than

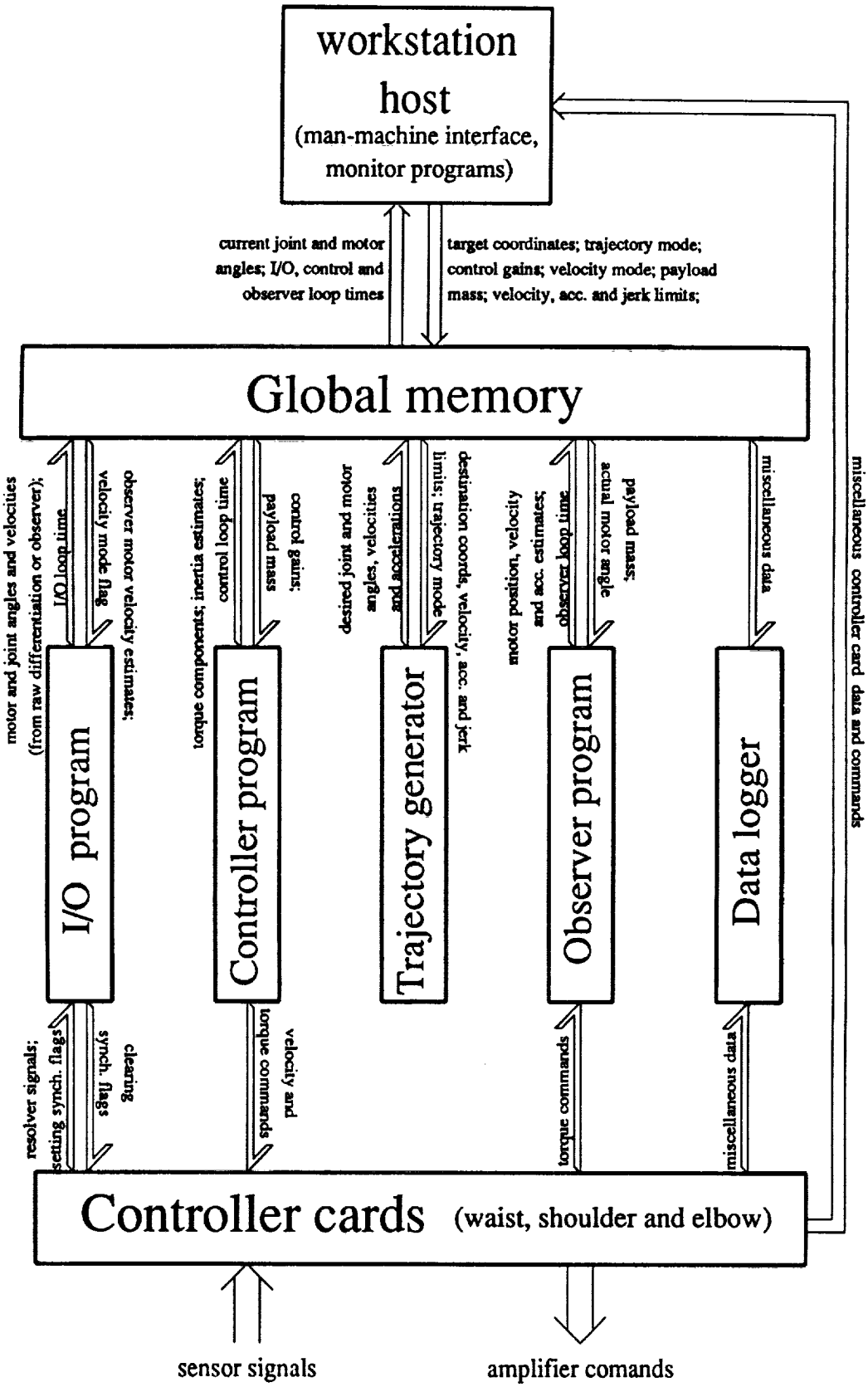

Figure 3: Data flow block diagram

what would be obtained through other means [17].

At present, the observer only works reliably during current control mode (see Section 5.1). It has not yet been fine-tuned for use in voltage control mode. This was partly due to the difficulty of accurately gauging the generated torques in this mode, and partly because velocity feedback is not currently used in voltage control mode.

This trajectory generator computes a smooth trajectory from the robot's current position to some target position. This can be done in either joint space or Cartesian space, subject to user-specified limitations on the velocities, accelerations and jerks. The constraints are imposed to increase the smoothness of the trajectory execution [16]. The computational complexity of the equations used was minimized [19], thus increasing the speed and accuracy of the trajectory generator [18].

4.2 Data logging software

The data logging software is similar to the four support modules in that they also run on a CPU board in the VME cage. They differ in that they are not necessary for operating the robot. However, they are useful for gathering data on various hardware and control variables as the robot is in operation. The logger samples various control-related variables and stores them in a MATLAB data file. This is explained in the report by Velasco [19].

4.3 Interface Programs

The man-machine interface is the program through which all user interaction occurs. Its operation is demonstrated in the report and video by Velasco and Newman [1, 19]. Among other things, it can be used to specify Cartesian or joint-space trajectories and impose jerk, acceleration and velocity limits. It also pre-tests each trajectory, to verify that it is physically permissible (e.g. will not cause collisions or violate joint angle limits).

In addition, the system boasts of a variety of interfaces for monitoring both hardware variables like bus voltage and motor temperature, and control parameters like desired positions and control gains.

5 Control System

5.1 Current Control

The original scheme for driving the motors involved current control. In response to torque commands from the software, the controller boards command the amplifiers to generate the required motor currents. This is done using motor current feedback and a servo control algorithm with proportional and integral gain. Based on this control law, the controller boards command the amplifiers to generate voltage pulses, or pulse width modulation (PWM) signals. These are used to make the motor currents converge to the desired values. In addition, the controller compensates for back-EMF effects by adding

an additional term to the PWM signals. This term is proportional to the motor velocity, and thus serves to counter the back-EMF voltage.

It was discovered, however, that the current sensing scheme led to problems with the current control algorithm. The controller boards sample the current readings at 8.0 kHz, while the PWM frequency is 15.63 kHz. Furthermore, the low phase inductances (79 μH) allow the currents to change quite drastically. (This is discussed further in Section 7.1.) As a result, the current readings are undersampled and do not provide a completely accurate measure of the motor currents. This is shown in Figure 4, where we see that the current sensor reading has strong oscillations. The vigorous current oscillations caused a grinding noise to issue from the motors whenever the robot was in motion.

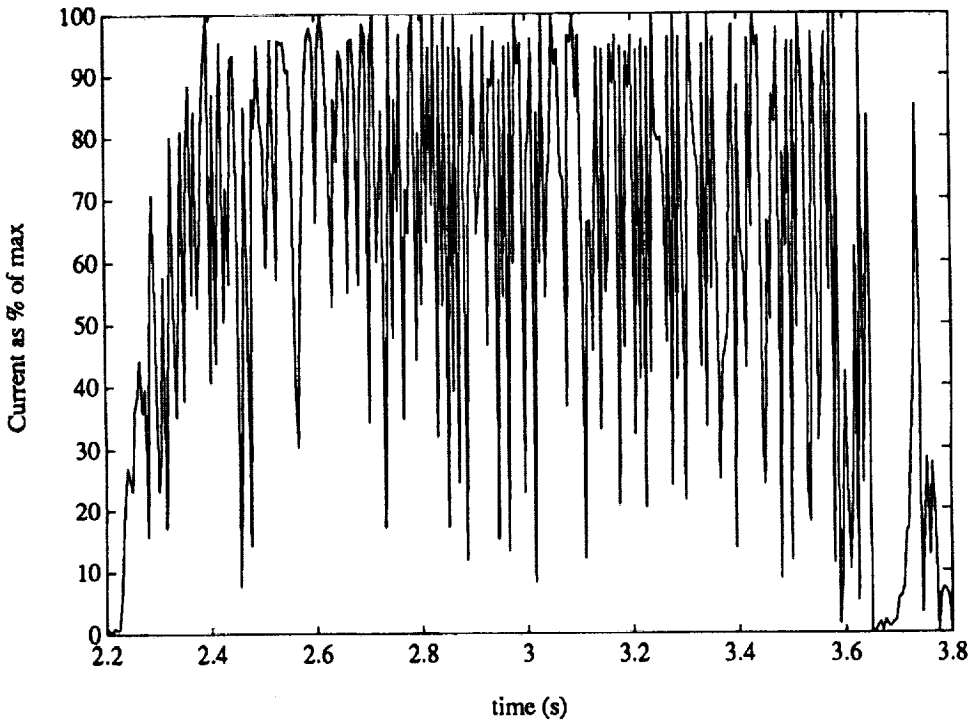

Figure 4: Elbow current readings under current control

5.2 Voltage control

To circumvent this problem, a new scheme was introduced to dispense with current feedback altogether. Instead of controlling the torques by modulating the motor currents, the boards controlled the velocities via the voltage pulses, with inherent back EMF performing equivalent velocity feedback [7, 15].

An additional PWM component is needed to generate a holding torque. This means that even when the arm is at rest, non-zero voltage pulses will be generated to prevent the arm from falling due to gravity. At zero velocity, this PWM component is proportional

to the desired torque. Under this scheme, the net PWM signal is simply the sum of the velocity-dependent and torque-dependent terms and does not rely on current feedback. (As discussed in Section 6 however, it turns out that this is not strictly true during current regeneration. Under certain circumstances, the programs on the DSP-based controller boards actually compute the velocity-dependent terms with some dependence on the torque command. By and large though, the description above is correct.)

5.3 Torque computation

Under current control, the servo control laws used were of the form

$$\begin{aligned} \tau_{n,servo} &= K_{p,n}(\theta_{n,des} - \theta_n) + K_{d,n}(\omega_{n,des} - \omega_n) + \\ &\quad K_{i,n} \int (\theta_{n,des} - \theta_n)\, dt \end{aligned} \tag{1}$$

where saturation limits were placed on the integrated error term on the right. In practice though, the integrator gains $K_{i,n}$ were set to zero because adding integral control caused oscillations in the final position. An explanation of this behavior is given in Section 7.2.

It proved useful to use two sets of control gains: one set of large gains when the joint velocity was greater than some tolerance, and smaller gains when the velocities are below some tolerance. Adjusting these gains on the fly increased the tracking accuracy at high velocities while preventing oscillations at lower speeds.

These servo torques were combined with feedforward torques to produce the net torque commands. These feedforward torques took into account ideal robot dynamics, gravity and friction.

Under voltage control, the net torque commands are simply given by

$$\tau_{n,servo} = K_{p,n}(\theta_{n,des} - \theta_n) \tag{2}$$

As of this writing, neither velocity feedback, integral feedback nor feedforward torques have yet been included. This is because the routines for switching between motor driving and current regeneration will require some fine-tuning before it will work in voltage control mode. This is because the current routines result in occasional amplifier dropouts along the trajectories. Thus, at the moment the desired torques are not accurately generated under voltage control and the observer does not yet produce reliable velocity estimates. The explanation behind these dropouts is given in Section 6.

6 Data and Results

The tracking accuracy was gauged using sinusoidal joint trajectories and straight-line paths in both joint and Cartesian space, for all three trajectory profiles. Due to various malfunctions in the prototype, however, only two working controller cards and two amplifiers were available, so the final tests could only be done on the shoulder and elbow.

In general, trajectory tracking under current control was very accurate, despite the noise and current oscillations. Figure 5 shows the results of a sample move done using

the elbow under current control. The joint angle follows the desired values very closely, with a maximum error of only 0.0104 radians. The precision would be improved if the PWM resolution were increased, as discussed in Section 7.

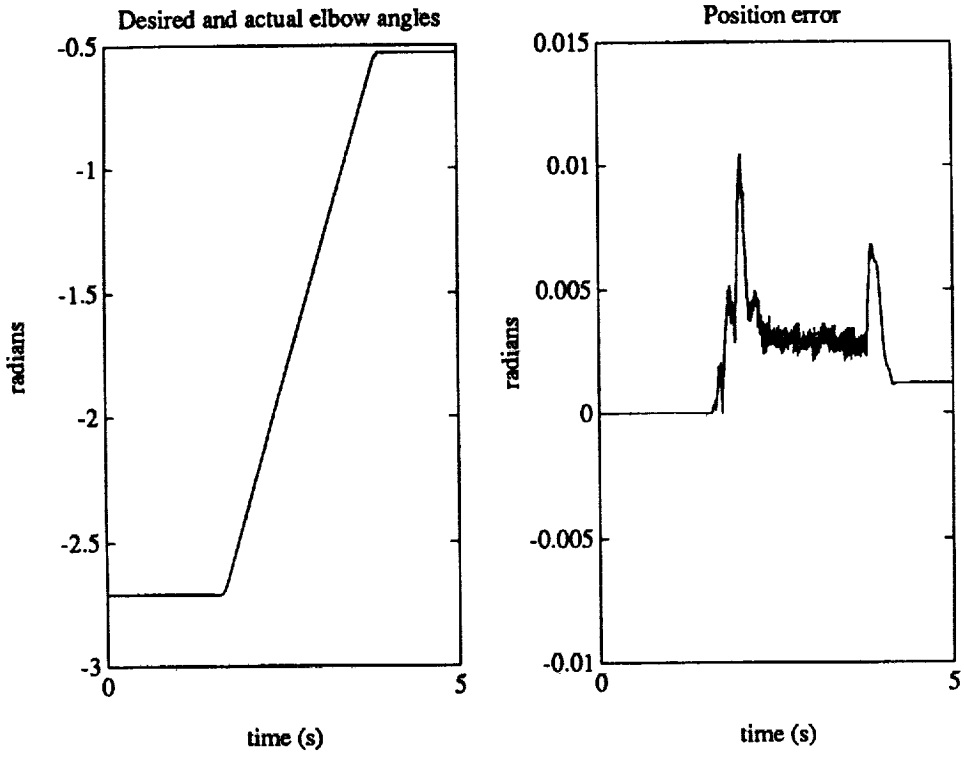

Figure 5: Elbow trajectory tracking under current control

Under voltage control, a bothersome high-speed amplifier switching noise was eliminated. However, Figure 6 shows that the tracking accuracy was not as high. The maximum position error is 0.0424 radians, and the error increases and decreases almost periodically. The decrease in accuracy is partly because of amplifier dropouts, and partly because the servo control gains were decreased to minimize the incidence of these dropouts.

The relationship between the amplifier dropouts and the trajectory tracking is shown in Figure 7. As can be seen from this and the previous plot, the PWM command drops to zero whenever the position error (and thus, the torque command) becomes negative. The cause of this behavior is explained in Section 7.3.

It is believed that when these problems are fixed, the tracking accuracy under voltage control would be comparable to, or greater than, that achieved with current control. It would permit the use of larger control gains, which should greatly increase the tracking accuracy. Tests show that when the position error gain is multiplied by twenty, the number of dropouts increases, but the maximum position error is 0.0234 radians—only about twice that achieved with current control. Without the amplifier dropouts, both the tracking accuracy and the final position error would doubtlessly be much smaller.

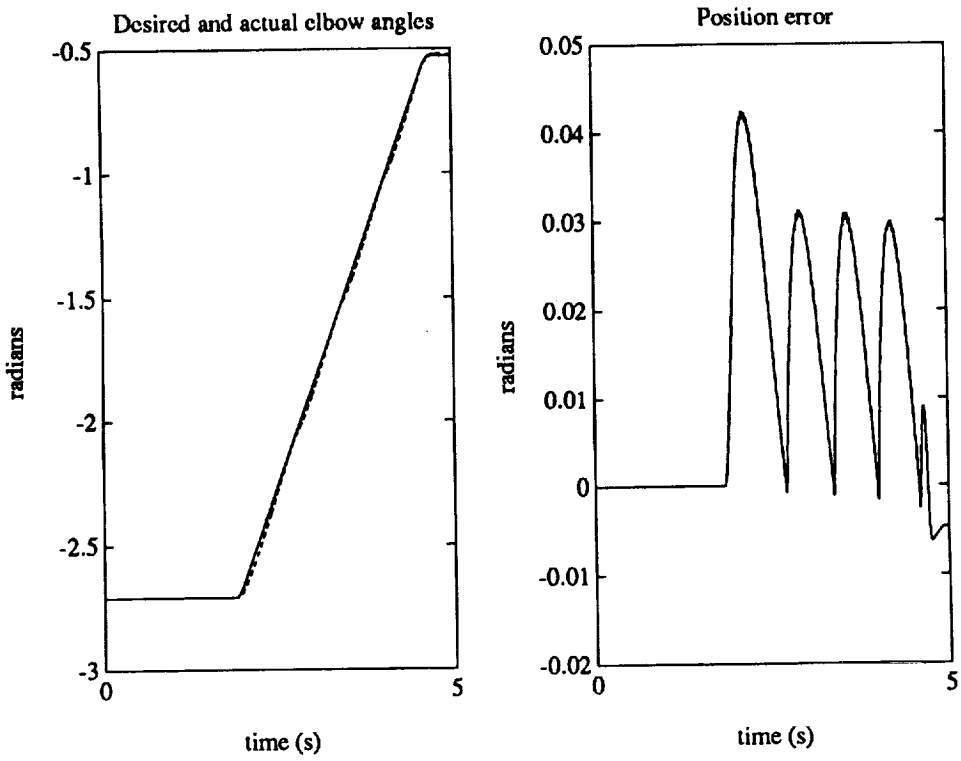

Figure 6: Elbow trajectory tracking under voltage control

7 Analysis

7.1 Current control vs. voltage control

As discussed in Section 6, the low motor inductances, while otherwise desirable, created complications by allowing the currents to change dramatically. At the design PWM frequency, the control hardware could not sample the current readings quickly enough to use them effectively in feedback. Computer simulations show that a single-phase excitation at the PWM frequency of 15.63 kHz and a 50% duty cycle would produce peak-to-peak current swings of up to 16 A. Since the current sensor only samples data at 8 kHz, it obtains a false profile of the actual current. This is aggravated when the profile is used in feedback, resulting in the vigorous high-frequency dynamics in Figure 4. These dynamics manifested themselves as a bothersome grinding noise and rapid position error oscillations [1, 19].

Implementing voltage control eliminated the bothersome noise and error oscillations which resulted from current control. It may be possible, however, to mitigate these effects by increasing the phase inductances. These inductances were kept small in order to achieve high-speed commutation; however, this was done at the expense of accurate current control. To avoid degrading the performance, one would want to maintain an effective stepping rate at the saturation velocity of 200 rad/s and the phase switching rate of 24 times per cycle. Computations show that the inductances can be comfortably

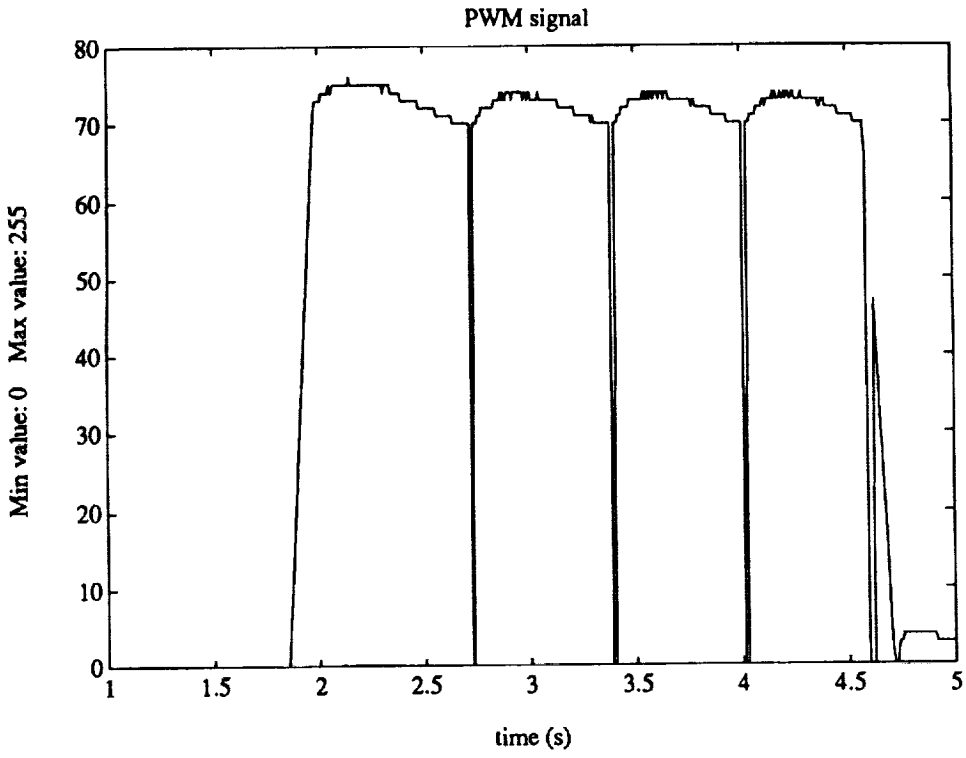

Figure 7: PWM signals for trajectory under voltage control

raised by about 270%. In practice, the inductance may have to be smaller than that, for fine commutation. Nevertheless, this estimate establishes an approximate upper limit to the inductances that can be used.

Increasing the PWM frequency should also reduce the size of the oscillations. In fact, computer modelling shows that by doubling the inductances and increasing the PWM frequency five-fold, the current oscillations can be reduced to one-tenth of their previous value. Similarly, position control error would be reduced as well.

7.2 PWM resolution

The PWM commands are linear combinations of a velocity-dependent term (which counters the back-EMF) and a torque-dependent term. These signals can assume any value from 0 to 255, where zero corresponds to no voltage and 255 corresponds to a duty cycle of 100%.

It was found that at zero velocity, the PWM count which corresponds to maximum torque is about 24. This limits the available torque resolution, and thus, the positioning accuracy. It also accounts for the oscillations that occured with integral error feedback (Section 5.3), and for the difficulties encountered in compensating for the friction. However, this problem can be addressed with some modest modifications to the control hardware.

7.3 Controller board routines

When the system was modified to accomodate voltage control, the resultant arm motion was very smooth, except that the amplifier would drop out on occasion. As shown in Section 6, this is because the PWM signal would drop down to zero whenever the controller board would switch into regeneration mode.

Close examination of the controller board program listing reveals why. Ordinarily, the PWM command is computed based on two terms: one torque-dependent, and one dependent on a velocity command. However during current regeneration, if the torque command is small enough, the second term is computed as being proportional to the commanded torque and inversely proportional to the velocity command. This creates two problems. One is that the PWM command actually decreases as the size of the velocity command increases. The other is that due to discretization errors, a small torque command may make the PWM signal small or even zero. These problems can be readily addressed via some modest changes to the PWM equations used by the controller board firmware.

8 Summary and Conclusions

As expected, the UNIQ motor outperformed other motors in its class. The motor's high power density, high torque to mass ratio and efficient heat dissipation, coupled with the compact, lightweight robot design provides many attractive features for space-based robot applications.

The comprehensive hardware and software developed for the robot permitted accurate trajectory tracking, flexibility and user-friendliness. However, the performance can be improved by modifying the controller board routines and by increasing the PWM frequency, the PWM resolution and the phase inductances.

9 Acknowledgements

This project was supported by a grant from the NASA/Lewis Research Center under contract NAS3-26285.

References

[1] Unique Mobility SBIR Phase II Final Report, Contract NAS3-26285.

[2] Gill, Richard Malcolm. *Carbon fibres in composite materials.* Iliffe Books for the Plastics Institute, London, 1972.

[3] Delmonte, John. *Technology of carbon and graphite fiber composites.* R. E. Krieger Publishing Company, Malabar, Florida, 1987.

[4] Sichel, Enid Keil. *Carbon black-polymer composites: the physics of electrically conducting composites.* M. Dekker, New York, 1982.

[5] Buckley, J. D. and Edie, D. D. *Carbon-carbon materials and composites.* Noyes Publications, Park Ridge, New Jersey, 1993.

[6] Parker, Sybil P., ed. *McGraw-Hill encyclopedia of engineering, second edition.* McGraw-Hill, Willard, Ohio, 1993.

[7] Krause, P. C. and Wasynczuk, O., *Electromechanical Motion Devices.* McGraw-Hill, New York, NY, 1989.

[8] Stanley, W. D., Dougherty, G. R. and Dougherty, R. *Digital Signal Processing.* Reston Pub. Co., Reston, Virginia, 1984.

[9] J. Ish-Shalom and P. Kazanzides. SPARTA: Multiple signal processors for high-performance robot control *IEEE Transactions on Robotics and Automation*, 5(5):628-640, 1989.

[10] Hwang, K. and Briggs, F. A. *Computer Architecture and Parallel Processing.* McGraw-Hill, New York, 1984.

[11] Newman, W. S., "The CAISR Mechatronics Lab Real-Time Multiprocessor System: Theory and Operation," Technical Report TR-89-144, Center for Automation and Intelligent Systems Research, Case Western Reserve University, Cleveland, Ohio, October 1989.

[12] Black, John, ed. *The System Engineer's Handbook: A Guide to Building VMEbus and VXIbus systems.* Academic Press, San Diego, 1992.

[13] H. Sira-Ramirez, M. Zribi and S. Ahmad. Pulse width modulation control of robotic manipulators. *International journal of systems science*, 24(8): 1423, 1993.

[14] Sarjeant, W. J. and Dollinger, R. E., *High-Power Electronics.* TAB Professional and Reference Books, Blue Ridge Summit, Pennsylvania, 1989.

[15] Bose, Bimal K., *Adjustable Speed AC Drive Systems.* IEEE Press, New York, NY, 1980.

[16] Brady, Michael, et al. *Robot Motion: Planning and Control.* The MIT Press, Cambridge, MA, 1984.

[17] Franklin, G. F., Powell, J. D., and Workman, M. L., *Digital Control of Dynamic Systems.* Addison-Wesley, New York, 2nd edition, 1990.

[18] Maron, Melvin J. *Numerical Analysis: A Practical Approach, 3rd ed..* Wadsworth Pub. Co., Belmont, California, 1991.

[19] Velasco, Virgilio B. Jr., "Characterization and Control of the Unique Mobility Corporation Robot Prototype" Technical Report TR-93-142, Center for Automation and Intelligent Systems Research, Case Western Reserve University, Cleveland, Ohio, December 1993.